JGR Oceans

RESEARCH ARTICLE
10.1029/2023JC020183

Time-Dependent Role of Multiyear La Niña in Impacting the Pacific Tropical Instability Waves

Wei-Bang He[1,2], Yang Yang[3], and X. San Liang[4,5,6]

[1]Department of Atmospheric Sciences, School of Ocean and Earth Science and Technology (SOEST), University of Hawai'i at Mānoa, Honolulu, HI, USA, [2]School of Marine Sciences, Nanjing University of Information Science and Technology, Nanjing, China, [3]State Key Laboratory of Marine Environmental Science, Department of Physical Oceanography, College of Ocean and Earth Sciences, Xiamen University, Xiamen, China, [4]The Artificial Intelligence Department, Division of Frontier Research, Southern Marine Laboratory, Zhuhai, China, [5]IRDR ICoE on Risk Interconnectivity and Governance on Weather/Climate Extremes Impact and Public Health, Fudan University, Shanghai, China, [6]CMA-FDU Joint Laboratory of Marine Meteorology, Department of Atmospheric and Oceanic Sciences, Institute of Atmospheric Sciences, Fudan University, Shanghai, China

Key Points:

- While the tropical instability wave (TIW) activity is believed to be enhanced by La Niña, in a multiyear La Niña, it is greatly decreased after the first year
- The decrease in TIW eddy kinetic energy (EKE) during the second-year La Niña is mainly due to a weakened baroclinic instability of the equatorial currents
- The spatial difference in the meridional structure of temperature pattern causes the difference in TIW EKE during multi-year events

Correspondence to:
X. S. Liang,
x.san.liang@gmail.com

Citation:
He, W.-B., Yang, Y., & Liang, X. S. (2024). Time-dependent role of multiyear La Niña in impacting the Pacific tropical instability waves. *Journal of Geophysical Research: Oceans*, *129*, e2023JC020183. https://doi.org/10.1029/2023JC020183

Received 28 JUN 2023
Accepted 3 DEC 2023

Abstract Previous studies have shown that the tropical instability waves (TIWs) in the Equatorial Pacific are enhanced during La Niña and suppressed during El Niño. Unlike El Niño which tends to decay quickly, La Niña often persists through the subsequent one or 2 years, becoming a multiyear La Niña. Using a time-dependent and space-localized energetics formalism and a suite of observational and reanalysis data, we found that the eddy kinetic energy (EKE) associated with TIWs only peaks during the first-year La Niña and decreases significantly during the second-year La Niña. This is caused, to the first order, by the weaker equatorial cold tongue near the equator and anomalous cooling in the off-equator regions during the second-year La Niña, as compared to the first-year La Niña, which leads to a significant decrease in meridional density shear, and thus a reduction in baroclinic instability. Meanwhile, the weakened South Equatorial Current during the second-year La Niña also contribute to EKE decrease by transferring less kinetic energy to the TIWs via barotropic instability. The meridionally broad spatial pattern of negative temperature anomalies during the second-year La Niña is the major reason for the weakened TIW activity.

Plain Language Summary Tropical Instability Waves (TIWs) are mesoscale waves propagating westward on edges of the equatorial Pacific cold tongue. Their interannual variability is strongly modulated by El Niño-Southern Oscillation, enhanced during La Niña and suppressed during El Niño years. In contrast to El Niño which tends to decay quickly, La Niña often persists through the subsequent one or two years, becoming a multiyear La Niña. For the first time, this study unveils the time-dependent feature of the TIW activity in the multiyear La Niña events. That is, the TIW activity, as measured by eddy kinetic energy, is largely weakened during the second-year La Niña as compared to the first-year La Niña. An energetics analysis reveals that baroclinic instability, a dominant energy source of the TIWs, is significantly weakened during the second-year La Niña. Meanwhile, the strength of barotropic instability (another major energy source of the TIWs) is also reduced. Our study indicates the importance of both baroclinic and barotropic instabilities in shaping the interannual evolution of TIWs during the multiyear La Niña.

1. Introduction

Tropical Instability Waves (TIWs) are oceanic mesoscale waves that develop in the equatorial Pacific and Atlantic. They propagate westward as cusp-like perturbations that ride on the sea surface temperature (SST) fronts on both sides of the equatorial cold tongue, and have a wavelength range of 1,000–2,000 km, a period range of 10–40 days, and a phase speed of ~0.5 m/s (Legeckis, 1977; Philander, 1978; Weisberg & Weingartner, 1988). In the equatorial Pacific, TIWs represent the primary source of mesoscale variability. It is found that TIWs are generated as a result of barotropic instability induced by the meridional velocity shear within the equatorial current system, and baroclinic instability induced by the temperature gradient within the temperature fronts on the northern side of the equatorial cold tongue (e.g., Masina et al., 1999; Qiao & Weisberg, 1998; Wang et al., 2020; Z. Yu et al., 1995). These instability processes are well connected to the thermodynamic structure of the eastern Pacific's equatorial cold tongue (J.-Y. Yu & Liu, 2003).

TIWs exhibit intense seasonal and interannual variations (Boucharel & Jin, 2019). Modulated by the seasonal cycles of the meridional velocity shear and temperature gradient near the equator, TIWs develop in the boreal ("boreal" will be omitted henceforth) summer and reach their peak during autumn and winter (Legeckis, 1977; Wang et al., 2017, 2019). On the interannual timescale, TIW activity is strongly modulated by the El Niño-Southern Oscillation (ENSO) (Boucharel & Jin, 2019), which is the dominant mode of the global interannual climate variability, oscillating between warm (El Niño) and cold (La Niña) phases. ENSO events generally develop in summer, peak in winter, and decay in the spring of the following year. During the developing year of La Niña events, the activity of TIWs is more intense due to the strengthened equatorial cold tongue, enhancing the meridional temperature gradient and thus making the background flow more baroclinically unstable. The opposite is true during El Niño events (An, 2008; Contreras, 2002; Yang & Liang, 2019; J.-Y. Yu & Liu, 2003).

Previous studies have shown that TIWs do not just respond passively to the background ocean state. Strong feedbacks from TIWs on the mean state and seasonal cycle of the eastern Pacific Ocean have been identified (Hansen & Paul, 1984; Imada & Kimoto, 2012; Jochum et al., 2007; Maillard, Boucharel, Stuecker, et al., 2022; Menkes et al., 2006). For instance, TIWs act to warm up the cold tongue and reduce the meridional temperature gradient by equatorward heat flux (Hansen & Paul, 1984; Jochum et al., 2007; Menkes et al., 2006). They also reduce the mean strength of the Equatorial Undercurrent (EUC), which results in a cooling effect that partly counterbalances the warming effect provided by the anomalous TIW-induced heat flux (Maillard, Boucharel, & Renault, 2022). In addition, recent studies reported that the TIW-induced warming effect tends to be stronger during La Niña than El Niño. This asymmetric feedback may be responsible for the ENSO amplitude asymmetry (e.g., An, 2008; Vialard et al., 2001).

In contrast to El Niño events which usually persist for 1 year, La Niña events tend to persist through the subsequent one or 2 years and often re-intensify during the subsequent winters (e.g., DiNezio & Deser, 2014; Hu et al., 2014; Kessler, 2002; Ohba & Ueda, 2009; Okumura et al., 2011). Previous studies have shown that multiyear La Niña events account for 35%–50% of total La Niña events (e.g., Okumura & Deser, 2010). These events can bring different climate impacts during their different periods (e.g., Okumura et al., 2017; Zhu & Yu, 2022). The thermodynamic structure of the equatorial cold tongue is quite different between the first-year La Niña and the second-year La Niña when a multiyear La Niña occurs (Feng et al., 2015; Hu et al., 2014; Park et al., 2021; Wu et al., 2019; Zheng et al., 2015). Anomalous cool water persists in the near-surface layer of off-equator regions of the eastern Pacific in the second year, which is not observed in the first year. This leads to a weaker meridional temperature gradient in the eastern Pacific during the second year compared to the first year (Chen et al., 2022; Geng et al., 2023). In addition, Hu et al. (2017) observed that the South Equatorial Current (SEC) is weaker during the second year compared to the first year. As the development of TIWs is controlled by the meridional temperature gradient and velocity shear, it is expected that the differences in the cold tongue and the equatorial current system can impact the generation of TIWs during the different years of the multiyear La Niña event. This motivates us to conjecture that a multiyear La Niña may impact the TIWs in a way different from a single-year La Niña.

So far, how multiyear La Niña events modulate the interannual TIW activities remains unclear. This study aims to address this issue, using a functional analysis tool, multiscale window transform (MWT) (Liang & Anderson, 2007), and the canonical transfer theory (Liang, 2016). We begin by introducing the methodology and data in Section 2, followed by a demonstration of the distinctly different influences on the TIW activities in different developing years exerted by the multiyear La Niña events (Section 3). The study is summarized and discussed in Section 4.

2. Method and Data

2.1. Quantification of Instability Energy Pathways

The main goal of this study is to quantify the two main energy pathways responsible for generating the TIWs, namely, the barotropic instability energy pathway (BT, kinetic energy transfer from the background flow scale to the TIW scale) and the baroclinic instability energy pathway (BC, potential energy transfer from the background flow scale to the TIW scale, and then converted into kinetic energy on the TIW scale). To achieve this, first, we need to separate the background flow and TIW perturbations from the raw signals. The classical formalism (e.g., Lorenz, 1955; von Storch et al., 2012) based on Reynolds mean-eddy decomposition does not work here

because it is formulated with temporal (or zonal) averaging and hence is inappropriate to investigate energy burst processes such as the TIW formation. A common practice in the literature in remedying this is to use filters. For instance, a velocity field $u(t)$ can be filtered into two components, that is, $u(t) = u'(t) + \overline{u}(t)$, in which $u'(t)$ represents the eddy component and $\overline{u}(t)$ represents the background component (also time-dependent). A fundamental but somehow overlooked question arises: what is the energy of the filtered field? It is very common in the literature to use $\left[\overline{u}(t)\right]^2$ and $\left[u'(t)\right]^2$ (up to some constant) as the energy of the background and eddy components. This practice is problematic because $\left[\overline{u}(t)\right]^2 + \left[u'(t)\right]^2$, that is, the total energy is not conserved. A simple example of the multiscale energy representation problem is shown in the appendix of Yang and Liang (2019). In fact, multiscale energy is a concept in phase space, such as that in the Fourier power spectrum. It is connected to physical energy by the Parseval's theorem.

To tackle the above problem, Liang and Anderson (2007) developed the MWT, a functional analysis tool that allows for a decomposition of signals onto several mutually orthogonal subspaces (referred to as scale windows ϖ hereafter) while retaining their localized (i.e., time-dependent) information. For a set of specially designed orthogonal filters, Liang and Anderson (2007) found that a pair of transform coefficient and reconstruction exists, just analogous to the Fourier transform and its inverse. The reconstruction is just like the conventional filter, while the transform coefficient, defined in the phase space, allows for a faithful representation of the energy on a certain scale window. Liang and Anderson (2007) proved that the energy on a scale window ϖ is proportional to the square of the transform coefficient, that is, $(\hat{u}_n^{\varpi})^2$, where $\widehat{(\cdot)}_n^{\varpi}$ is the MWT operator (n denotes the discrete time step).

Using MWT, we decompose the original fields into three orthogonal scale windows, namely, a background flow window (with periods >48 days), a TIW window (with periods 12–48 days), and a high-frequency (submesoscale) window (with periods <12 days), which are denoted by $\varpi = 0, 1, 2$, respectively. The definition of the TIW window is based on the major period of TIWs (Lyman et al., 2007; Qiao & Weisberg, 1995, 1998), and is consistent with our previous study that analyzes the TIW energetics using MWT (He et al., 2023). Using the MWT transformed coefficients, the multiscale KE and the available potential energy (APE) are

$$K^{\varpi} = \frac{1}{2}\rho_0 \hat{\boldsymbol{u}}_h^{\varpi} \cdot \hat{\boldsymbol{u}}_h^{\varpi}, \tag{1}$$

and

$$A^{\varpi} = \frac{C}{2}\left(\hat{\rho}^{\varpi}\right)^2, \tag{2}$$

respectively, where $\boldsymbol{u}_h$ is the horizontal velocity, $\rho_0 = 1\ 025\ \mathrm{kg\ m^{-3}}$ is the reference density of seawater, and ρ is the density perturbation from a background reference profile $\overline{\rho}(z)$, that is, the time- and area- mean of the original density field at each depth, $C = \frac{g^2}{\rho_0{}^2 N^2}$ ($N = \sqrt{-\frac{g}{\rho_0}\frac{\partial \overline{\rho}}{\partial z}}$, $g = 9.8\ \mathrm{m\ s^{-2}}$).

Based on MWT, BT and BC can be quantitatively described by the cross-scale transfer of KE and APE from the background flow window to the TIW window (Liang & Anderson, 2007). As proved in Liang (2016), the cross-scale KE and APE transfers are given by:

$$\Gamma_K^{\varpi} = \frac{\rho_0}{2}\left[\widehat{(\boldsymbol{u}\boldsymbol{u}_h)}^{\varpi} : \nabla \hat{\boldsymbol{u}}_h^{\varpi} - \nabla \cdot \widehat{(\boldsymbol{u}\boldsymbol{u}_h)}^{\varpi} \cdot \hat{\boldsymbol{u}}_h^{\varpi}\right] \tag{3}$$

and

$$\Gamma_A^{\varpi} = \frac{C}{2}\left[\widehat{(\boldsymbol{u}\rho)}^{\varpi} \cdot \nabla \hat{\rho}^{\varpi} - \hat{\rho}^{\varpi} \nabla \cdot \widehat{(\boldsymbol{u}\rho)}^{\varpi}\right], \tag{4}$$

respectively, where the colon ":" is the double-dot product of two dyads.

The above transfer matrices follow a conservation law:

$$\sum_n \sum_{\varpi} \Gamma_n^{\varpi} = 0, \tag{5}$$

which indicates that the sum of cross-scale transfers over all sampling time steps n and windows ϖ is equal to 0. [The subscript n is omitted in the aforementioned equations for simplicity]. This property suggests that these transfers neither produce nor consume energy; their sole function is the redistribution of energy within the phase

(frequency) space. It is worth noting that this seemingly fundamental property does not hold in other traditional energetics formalisms. To distinguish, Γ^{ϖ} is referred to as "canonical transfer" (Liang, 2016).

Note that the canonical transfers in Equations 3 and 4 should be further decomposed to pick out the window-window interactions within our three-scale window framework. This is fulfilled by the "interaction analysis" as illustrated in Liang and Robinson (2005). The following briefly describes the procedure. Note that Γ^{ϖ} is just a linear combination of some triple product terms like

$$\Gamma^{\varpi} = \widehat{\mathfrak{R}}^{\sim\varpi}\left(\widehat{pq}\right)^{\sim\varpi}. \tag{6}$$

It can be decomposed, taking the TIW window ($\varpi = 1$) for example, as:

$$\begin{aligned}\Gamma^{1} = \widehat{\mathfrak{R}}^{\sim 1}\left(\widehat{pq}\right)^{\sim 1} &= \widehat{\mathfrak{R}}^{\sim 1}\left(\sum_{\varpi_1=0}^{2} \widehat{p^{\sim\varpi_1}} \sum_{\varpi_1=0}^{2} q^{\sim\varpi_1}\right)^{\sim 1} \\ &= \underbrace{\widehat{\mathfrak{R}}^{\sim 1}\left[\left(\widehat{p^{\sim 0}q^{\sim 0}}\right)^{\sim 1} + \left(\widehat{p^{\sim 0}q^{\sim 1}}\right)^{\sim 1} + \left(\widehat{p^{\sim 1}q^{\sim 0}}\right)^{\sim 1}\right]}_{\Gamma^{0\to 1}} \\ &\quad + \underbrace{\widehat{\mathfrak{R}}^{\sim 1}\left[\left(\widehat{p^{\sim 1}q^{\sim 2}}\right)^{\sim 1} + \left(\widehat{p^{\sim 2}q^{\sim 1}}\right)^{\sim 1} + \left(\widehat{p^{\sim 2}q^{\sim 2}}\right)^{\sim 1}\right]}_{\Gamma^{2\to 1}} \\ &\quad + \underbrace{\widehat{\mathfrak{R}}^{\sim 1}\left[\left(\widehat{p^{\sim 0}q^{\sim 2}}\right)^{\sim 1} + \left(\widehat{p^{\sim 2}q^{\sim 0}}\right)^{\sim 1}\right]}_{\Gamma^{0\oplus 2\to 1}} + \underbrace{\widehat{\mathfrak{R}}^{\sim 1}\left[\left(\widehat{p^{\sim 1}q^{\sim 1}}\right)^{\sim 1}\right]}_{\Gamma^{1\to 1}}.\end{aligned} \tag{7}$$

On the right side of the Equation 7, the first term $\Gamma^{0\to 1}$ represents the energy transfer from the background flow window ($\varpi = 0$) to the TIW window. A positive $\Gamma_K^{0\to 1}$ indicates a KE transfer to the TIW window from the background flow window via BT (i.e., $K^0 \to K^1$). The APE stored in the background flow window can be released to the TIW window, and then converted to the TIW-scale KE (hereafter referred to as TIW EKE for brevity) through BC (i.e., $A^0 \to A^1 \to K^1$), where a positive APE transfer $\Gamma_A^{0\to 1}$ represents an APE transfer from the background flow window to the TIW window ($A^0 \to A^1$) and a positive buoyancy conversion $-b^1$ (expressed as $-g\widehat{\rho}^{\sim\varpi}\widehat{w}^{\sim\varpi}$) signifies the conversion from the TIW APE to the TIW EKE ($A^1 \to K^1$). However, in Equation 4, the quasi-geostrophic definition of APE has been adopted, which may not provide sufficient accuracy for the near-surface layer where TIWs are concentrated, as intense density perturbation along with weak stratification exists in this layer. So in evaluating $\Gamma_A^{0\to 1}$, Equation 4 may not be accurate enough. We hence, instead, use $-b^1$ (i.e., the second phase of BC) to make the inference of the baroclinic instability pathway, following He et al. (2023). Therefore, in this study, the strength of TIW activity, BT, and BC are quantitatively described by K^1, $\Gamma_K^{0\to 1}$, and $-b^1$, respectively. But caution should be used here, since in general $-b^1$ may be quite different from $\Gamma_A^{0\to 1}$ (see, e.g., Liang & Robinson, 2004).

In this study, we introduce the high-frequency window ($\varpi = 2$) to separate TIW signals from the submesoscale signals in the eastern tropical Pacific Ocean, as was done in our previously published paper (He et al., 2023). In that study, we have shown that the energy transfer between the TIW and the submesoscale variability ($\Gamma^{2\to 1}$) is negligible compared to that between the TIW variability and the background flow ($\Gamma^{0\to 1}$), suggesting that the high-frequency submesoscale variability is not likely to have a significant influence on the TIW activity. In addition, the $\Gamma^{0\oplus 2\to 1}$ and $\Gamma^{1\to 1}$ terms in Equation 7 are negligibly small. Therefore, these three terms $\Gamma^{2\to 1}$, $\Gamma^{0\oplus 2\to 1}$, and $\Gamma^{1\to 1}$ will not be considered in this study.

2.2. Data

Monthly $1^\circ \times 1^\circ$ SST data is distributed by Hadley Center sea ice and sea surface temperature (HadISST; Rayner et al., 2003) is used for the period 1993–2022. In the absence of geostrophic balance within the equatorial band, geostrophic surface currents derived from satellites often lead to an underestimation of the TIW signal near the equator, as noted in previous studies (He et al., 2023; Tuchen et al., 2018). Furthermore, certain variables

essential for analyzing the generation mechanisms of TIWs, such as vertical velocity and density, are not provided by the observation. To overcome these limitations, we use outputs from the daily 1/12° Global Ocean Physics Reanalysis (GLORYS12V1) for the period 1993–2020 from Copernicus Marine and Environment Monitoring Service (CMEMS) (Jean-Michel et al., 2021). We will refer to this data set as GLORYS hereafter. The GLORYS product has 50 levels in the vertical. Since the TIW signals are concentrated in the near-surface layer, we use only the top 28 levels spanning the 0–300 m depth range. It is worth noting that the comparison between different oceanic reanalysis data sets has shown that GLORYS can realistically simulate the TIW activity in the equatorial Pacific (Xue et al., 2023). Daily global surface geostrophic current data from the Archiving, Validation, and Interpretation of Satellite Oceanographic Data (AVISO) on a $1/4^{\circ} \times 1/4^{\circ}$ grid is used for the period 1993–2022. This data set is derived from the observations of multiple satellite altimeters (Traon et al., 1998) and will be referred to as AVISO hereafter. We use AVISO to validate the results from GLORYS and examine the latest multiyear La Niña event (2020–2022).

2.3. Definition of the Multiyear La Niña

The Niño-3.4 index is the SST anomaly averaged over the region 170°W–120°W and 5°S–5°N from HadISST. A La Niña event is defined when a 5-month moving average of the Niño-3.4 index is lower than or equal to −0.5°C in a period longer than 5 months. A multiyear La Niña event is defined as two La Niña events occurring during two consecutive winters. During the period 1993–2023, five multiyear La Niña events (1998–2001, 2007–2009, 2010–2012, 2016–2018, 2020–2023) are identified. These results are consistent with the La Niña years observed in the Oceanic Niño Index provided by NOAA (https://origin.cpc.ncep.noaa.gov/products/analysis_monitoring/ensostuff/ONI_v5.php). We refer to the first developing year of each multiyear La Niña event (1998, 2007, 2010, 2016, 2020) as the first year, and the second La Niña developing year (1999, 2008, 2011, 2017, 2021) as the second year. For the 1998–2001 and 2020–2023 multiyear La Niña events which persisted for 3 years, we only consider the first 2 years (1998–2000 and 2020–2021), as the similarity between the second and third years of the multiyear La Niña event is still controversial and thus previous multiyear ENSO studies generally only considered the first 2 years (e.g., Park et al., 2021; Wu et al., 2019). Note that due to the time limit of the GLORYS data set, the latest multiyear La Niña event (2020–2022) is only considered in the results using HadISST and AVISO.

3. Results

3.1. Background State

We first examine differences between the SST patterns in the TIW active season (June–February) of the first and second years of the multiyear La Niña events during 1993–2022. In addition to the common feature of the La Niña phenomenon, that is, the anomalous SST cooling over the equatorial Pacific, composite maps of the SST anomalies capture the contrast between the different years (Figure 1). The key difference appears in the meridional distribution of the SST anomalies. During the first year, the development of the anomalous SST cooling is restricted to the equatorial region in summer (June-July-August, JJA) and autumn (September-October-November, SON) (Figures 1a1 and 1a2). In contrast, during the second year, the anomalous SST cooling is more meridionally widespread, affecting off-equator regions in the same seasons (Figures 1b1 and 1b2). As a result, the meridional SST gradient in the equatorial eastern Pacific is weaker during the second year compared to the first year. The above description is consistent with previous studies (Chen et al., 2022; Feng et al., 2015; Geng et al., 2023; Hu et al., 2014; Park et al., 2021; Zheng et al., 2015). In winter (December-January-February, DJF), the difference in the meridional SST gradient is no longer evident, but the SST east of 120°W is cooler during the second year compared to the first year (Figures 1a3 and 1b3).

Next, we investigate the differences between the first and second years of the multiyear La Niña events during 1993–2018 in the equatorial cold tongue and current system by depicting depth-latitude distributions of the composited density and zonal velocity anomalies, respectively. Between 0 and 160 m, the long-term mean density on the equator is larger than that on both sides of the equator (Figures 2a1–2b3), revealing the cold tongue on the equator and the thermocline troughs on both sides of the equator (Wang et al., 2017). Throughout the first year, the density in the first 160 m is strengthened at the equator (Figures 2a1–2a3), consistently with the anomalous SST cooling restricted to the equatorial region (Figures 1a1–1a3), indicating a strengthening of the cold tongue. In contrast, during the summer of the second year, the density is strengthened on both sides of the equator

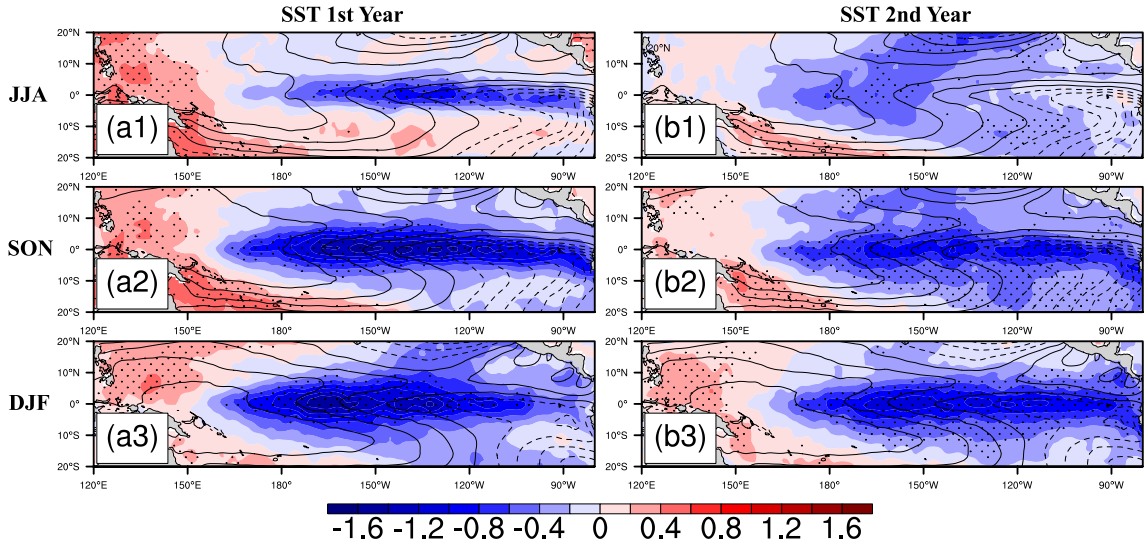

Figure 1. Composites of the sea surface temperature (SST) anomalies from HadISST (shadings, °C) for (a1–a3) the first and (b1–b3) second years of the multiyear La Niña events during 1993–2022 in (a1 and b1) June-July-August, (a2 and b2) September-October-November, and (a3 and b3) December-January-February. The long-term mean SST is superimposed, with solid contours above or equal to 26°C and dashed contours below 26°C (contour interval: 1°C). Hatched areas are significant at the 95% confidence level.

(Figure 2b1), consistently with the anomalous SST cooling over the off-equator regions (Figure 1b1). Furthermore, in the autumn and winter of the second year, the positive density anomalies in the first 80 m are stronger on both sides of the equator and weaker on the equator (Figures 2b2 and 2b3) compared to the first year (Figures 2a2 and 2a3). The distributions of the density anomalies during the second year reflect a relatively weak equatorial cold tongue and a weakened thermocline trough on the north side of the equator. This is due to the anomalous surface and subsurface cool water persisting in the off-equator region of the tropical eastern Pacific only during the second year, which is the signal of the westward Rossby wave reflected at the oceanic eastern boundary in the winter of the first year (Feng et al., 2015; Hu et al., 2014; Park et al., 2021; Wu et al., 2019; Zheng et al., 2015).

The long-term mean zonal velocity is positive on the equator between 40 and 200 m (Figures 2c1–2c3 and 2e), corresponding to the eastward EUC, while the negative velocity on both sides of the equator between 0 and 100 m corresponds to the westward SEC (Figures 2c1–2c3 and 2e). North of the equator, the long-term mean zonal velocity is positive between 4°N–9°N and 0–120 m, corresponding to the eastward North Equatorial Countercurrent (NECC) (Figures 2c1–2c3 and 2e). In the summer, autumn, and winter of both the first and second years, there are significant positive zonal velocity anomalies near the EUC (Figures 2c1–2c3 and 2d1–2d3), indicating that the EUC is strengthened. In the summer and autumn of the first year and the autumn of the second year, there are significant negative zonal velocity anomalies about the SEC (especially the northern branch of SEC) and between the northern branch of SEC (nSEC) and NECC (Figures 2c1, 2c2, and 2d2), suggesting that SEC is strengthened and the nSEC is shifted northward. During the first year, the positive zonal velocity anomalies about the EUC and the negative zonal velocity anomalies about the nSEC are stronger in summer and autumn (Figures 2c1 and 2c2) than those during the second year (Figures 2d1 and 2d2), representing that the EUC and nSEC are more strengthened. In the winter of both the first and second years, only the EUC is significantly strengthened (Figures 2c3 and 2d3); and there are still negative zonal velocity anomalies between the nSEC and NECC, suggesting that the nSEC is still abnormally far north (Figures 2c3 and 2d3). Besides, the EUC is still stronger in the winter of the first year (Figure 2c3) compared to the second year (Figure 2d3). As the nSEC is trapped in the equatorial front between the equatorial cold tongue and the thermocline trough in thermal–wind balance (Wang et al., 2017), the weaker meridional density gradient across the equatorial front in the summer and autumn of the second year can explain the weakening of the nSEC. The strengthening of trade winds during La Niña drives an enhanced zonal wind stress over the western and central equatorial Pacific (Izumo, 2005), which can explain the strengthening of the EUC (Figures 2c1–2c3 and 2d1–2d3) as the EUC is driven by the integrated wind stress over the equatorial Pacific (McPhaden, 1993). It is expected that the differences in the equatorial current system and cold tongue can impact the generation of TIWs.

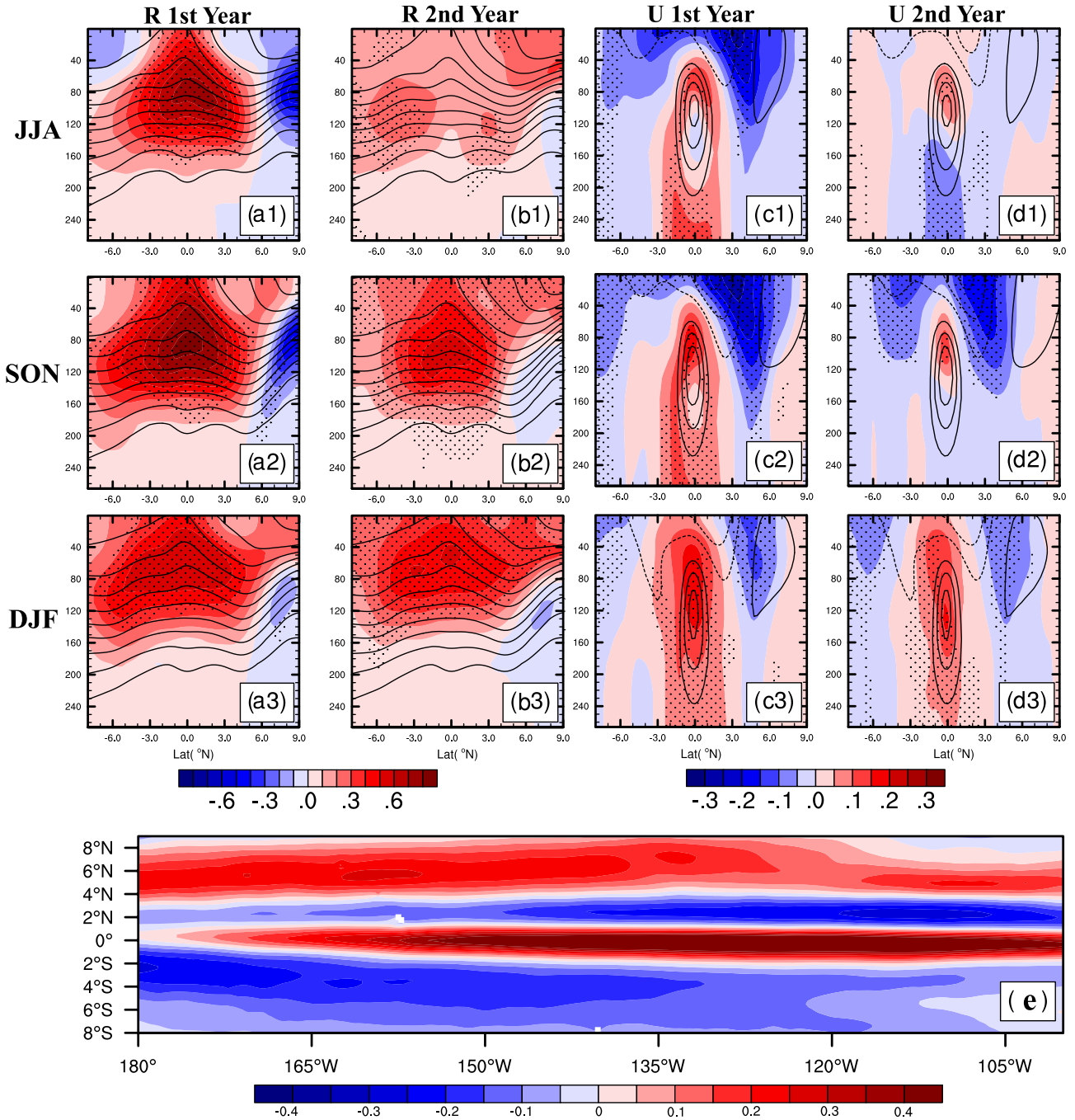

Figure 2. (a1–b3) The depth-latitude distributions of the composited density anomalies (ρ, shadings, kgm^{-3}) averaged across 180°–100°W for (a1–a3) the first and (b1–b3) second years of the multiyear La Niña events during 1993–2018 based on GLORYS. (c1–d3) As in (a1–b3), but for the zonal velocity anomalies (u, shadings, ms^{-1}). The long-term mean density and zonal velocity are superimposed as solid and dashed contours for positive and negative values on (a1–b3) and (c1–d3), with contour spacing of 0.5 kgm^{-3} and 0.2 ms^{-1}, respectively. Hatched areas are significant at the 95% confidence level. (e) Horizontal distribution of the annual mean zonal velocity (u, shadings, ms^{-1}) averaged vertically between the surface and 150 m.

3.2. TIW EKE and Its Sources

We compare the anomalous TIW EKE (K^1) composited for the first and second years of the multiyear La Niña events during 1993–2018 respectively in Figures 3a1–3a3 and 3b1–3b3 as depth-latitude maps averaged in 180°–100°W. During the first year, the TIW EKE anomalies exhibit significantly positive values north of the equator extending vertically from the surface to more than 160 m from summer to winter (Figures 3a1–3a3).

Conversely, during the second year, the TIW EKE anomalies are slightly weakened in summer (Figure 3b1) and significantly positive in autumn and winter (Figures 3b2–3b3) but still weaker compared to the first year. These results suggest a feature of the multiyear La Niña that TIWs are more active during the first year compared to the second year. We further analyzed the sources of TIW EKE to uncover the cause of such a feature in TIW activity during the multiyear La Niña.

Regard to the sources of TIW EKE, that is, BT ($\Gamma_K^{0\to1}$), and BC ($-b^1$), the background flow is more barotropically and baroclinically unstable during the first year, promoting the anomalous generation of TIWs, as seen in the substantial positive BT and BC anomalies north of the equator from summer to winter (Figures 3c1–3c3 and 3e1–3e3), compared to the weaker positive BT and BC anomalies in the same period of the second year (Figures 3d1–3d3 and 3f1–3f3), respectively. The strengthened BT during the first year is located between the NECC and the enhanced nSEC, suggesting that it is caused by the strengthened meridional velocity shear that is produced by the anomalously enhanced and northward nSEC (Figures 2c1–2c3). The enhanced BC during the first year is located between the cold tongue and thermocline trough north of the equator, suggesting that it is caused by the increased meridional temperature shear on the north edge of the strengthened cold tongue (Figures 1a1–1a3 and 2a1–2a3), while the relatively attenuated BC during the second year is caused by the decreased meridional temperature shear between the weaker equatorial cold tongue and the weakened thermocline trough (Figures 1b1–1b3 and 2b1–2b3). During the first year, the positive anomalies of BT are concentrated from the surface to 40–60 m (Figures 3c1–3c3), while those of BC are concentrated from 10 m to 160–200 m (Figures 3e1–3e3). This suggests that the BT anomalies favor the TIW anomalies near the surface, while the BC anomalies favor the TIW anomalies in the subsurface.

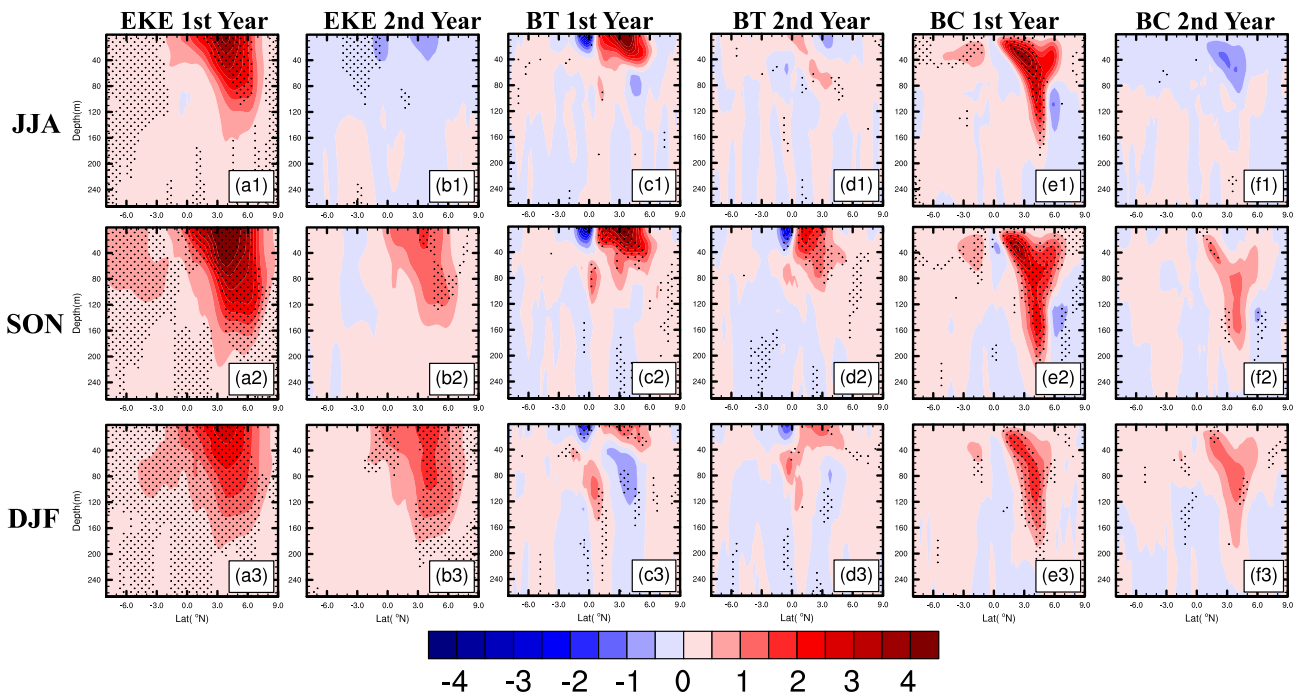

Figure 3. The depth-latitude distributions of the composites of the tropical instability wave eddy kinetic energy (shadings, $\times10^{-2}$m^2 s^{-2}) anomalies based on GLORYS averaged across 180°–100°W for (a1–a3) the first and (b1–b3) second years of the multiyear La Niña events during 1993–2018 based on GLORYS. (c1–d3) As in (a1–b3), but for the BT anomalies (shadings, $\times10^{-8}$m^2 s^{-3}). (e1–f3) As in (a1–b3), but for the BC anomalies (shadings, $\times10^{-8}$m^2 s^{-3}). Hatched areas are significant at the 95% confidence level.

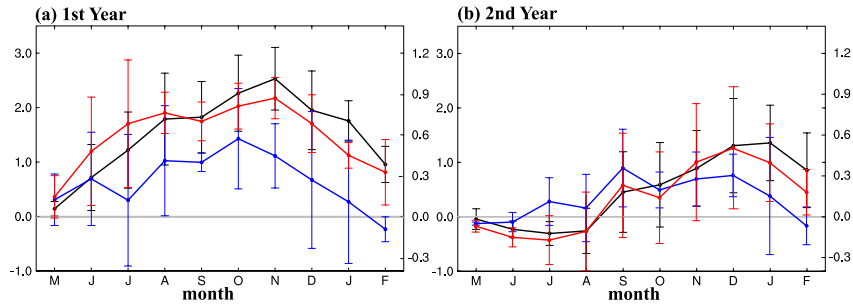

Figure 4. Composites of the tropical instability wave (TIW) eddy kinetic energy (EKE) (black lines; $m^3\ s^{-2}$), BT (blue lines; $\times10^{-6}\ m^3\ s^{-3}$), and BC (red lines; $\times10^{-6} m^3\ s^{-3}$) anomalies averaged over the eastern equatorial Pacific vertically integrated from the surface to 300 m for (a) the first and (b) second years of the multiyear La Niña events during 1993–2018 based on GLORYS. In each subplot, the ordinate for the TIW EKE is on the left-hand side, and that for other terms is on the right. The error bars represent the 95% confidence band.

One can see that most of the TIW EKE, BT, and BC anomalies exist only in the Northern Hemisphere. The weaker BT and BC south of the equator result respectively from a weaker branch of the SEC and a weaker temperature front on this side of the equator. Consequently, the TIW variability is also weakened (e.g., Hansen & Paul, 1984; Masina et al., 1999; Z. Yu et al., 1995).

The area-averaged and vertically integrated results reveal distinct characteristics of seasonality of the TIW EKE anomaly and its sources between the first and second years (Figure 4). During the first year, the TIW EKE anomaly exhibits significantly positive from June to February (Figure 4a). In contrast, during the second year, it is significantly negative from June to July and only becomes significantly positive from November to February (Figure 4b). This disparity indicates a notable difference in the seasonality of the TIW EKE anomaly between the first and second years. TIW activity is enhanced from summer to winter during the first year, while it is suppressed in summer and enhanced in autumn and winter during the second year. The TIW EKE anomaly presents a striking contrast between the summers of the first and second years. For instance, in July, the TIW EKE during the first year is 3.0 $m^3\ s^{-2}$, which is 1.8 times the long-term mean TIW EKE (1.7 $m^3\ s^{-2}$) and twice the TIW EKE during the second year (1.5$m^3\ s^{-2}$), suggesting the distinct difference of TIW activity between the first and second years. Furthermore, both the BT and BC anomalies are significantly positive in the autumn of the first year, confirming that both the BT and BC anomalies contribute to the enhanced TIW EKE. Notably, the BC anomaly exhibits significantly greater strength than the BT anomaly in summer and February, with its evolution more closely aligned with that of the TIW EKE anomaly. During the second year, the BC anomaly is significantly negative in June and positive in winter, also aligning more closely with the seasonality of the TIW EKE compared to the BT anomaly, suggesting that BC plays a crucial role in modulating the TIW EKE during the second year. Overall, these results indicate that BC is vital for the impact of the multiyear La Niña on the TIW EKE, and the disparity in the BC anomaly accounting for the divergent seasonality observed in the TIW EKE anomaly.

To make sure that the difference in TIW activity in the composites based on GLORYS reanalysis is not an artifact of a particular multiyear La Niña event, we compare the distribution of the surface TIW EKE (K^1) anomalies averaged over the TIWs active season (June-February) during the first and second years of every one of the multiyear La Niña events (Figure 5). Results from GLORYS reanalysis show positive TIW EKE anomalies over the eastern equatorial Pacific, especially north of the equator, for every year during the multiyear La Niña events (Figures 5a and 5b). This aligns with previous studies indicating enhanced TIW activity during La Niña (An, 2008; Contreras, 2002; J.-Y. Yu & Liu, 2003). However, for each multiyear La Niña event, the TIW EKE anomaly averaged over the eastern equatorial Pacific north of the equator, where the strongest TIW EKE anomalous signals exist during the multiyear La Niña (Figures 3a1–3a3 and 3b1–3b3), is stronger during the first year (1998, 2007, 2010, and 2016) compared to the second year (1999, 2008, 2011, and 2017). These results indicate that the difference in TIW activity over the years of a multi-year La Niña is a robust feature of the impact of the multi-year La Niña on TIWs, with TIWs being more active in the first year. Furthermore, this feature is also evident in the results from AVISO observations, demonstrating the fidelity of the GLORYS reanalysis (Figures 5c and 5d). The latest multiyear La Niña event (2020–2022), observable thanks to AVISO, produced similar results with TIW activity notable stronger in the first year than in the second. The possible reason for the negative TIW EKE anomaly during some second years such as 2021 is the abnormally weak BC. During these years, the meridional temperature gradient between the weaker equatorial tongue and the anomalously weakened thermocline trough may be too weak to reach its long-term mean amplitude,

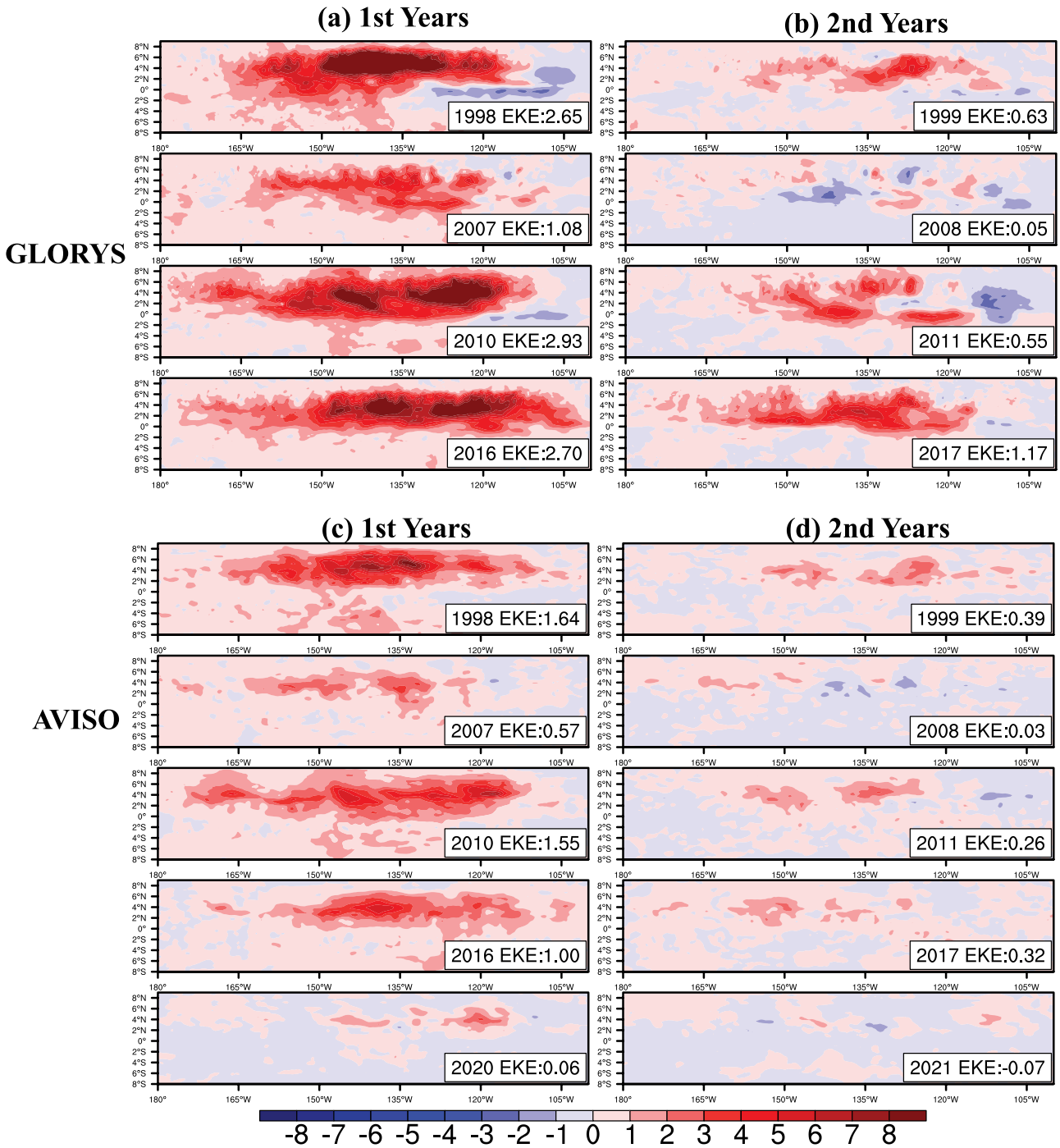

Figure 5. (a)–(b) Spatial distribution of the surface tropical instability wave (TIW) eddy kinetic energy (EKE) anomalies (shadings, $\times 10^{-2} m^2 s^{-2}$) based on GLORYS averaged over June through February for (a) all the first and (b) second years of the multiyear La Niña events during 1993–2018. (c)–(d) are the same as (a)–(b) but based on Archiving, Validation, and Interpretation of Satellite Oceanographic Data for (c) all the first and (d) second years of the multiyear La Niña events during the period 1993–2022. The label on each subplot denotes the surface TIW EKE anomaly averaged over the region 180°–100°W and 0°–9°N for each year.

resulting in the abnormally suppressed BC. As the major source for the TIW EKE anomalies, the abnormally weak BC can lead to the abnormally weak TIW EKE. Note that the TIW EKE anomalies from GLORYS are always stronger than those from AVISO, which is attributed to the satellite-based geostrophic surface current underestimating the TIW EKE near the equator where geostrophic balance is absent (He et al., 2023; Tuchen et al., 2018).

Comparing the time series of Niño-3.4 index (Figure 6a) and the area-averaged surface TIW EKE anomaly (Figure 6b) shows that TIWs are more active during the first year of a multiyear La Niña event, regardless of the

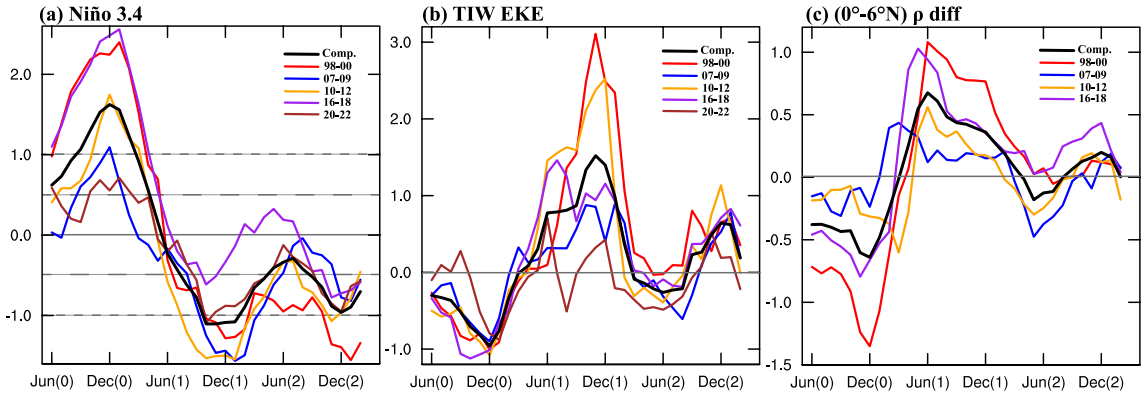

Figure 6. (a) Time series of Niño-3.4 index (°C) from June(0) to February(2) for the multiyear La Niña events during 1993–2022 based on HadISST, with the black thick line being a composite time series. The dashed horizontal lines at ±0.5°C denote the threshold of El Niño-Southern Oscillation (ENSO) events, and the lines at ±1°C denote the threshold of strong ENSO events. (b) is the same as (a) but for the surface tropical instability wave eddy kinetic energy anomaly ($\times 10^{-2} m^2 s^{-2}$) averaged over the region 180°–100°W and 0°–9°N for the multiyear La Niña events during 1993–2022 based on Archiving, Validation, and Interpretation of Satellite Oceanographic Data. (c) is the same as (a) but for the density difference anomaly (kgm^{-3}) between 0° and 6°N averaged over 180°–100°W and 0–50 m for the multiyear La Niña events during 1993–2018 based on GLORYS. Note that (0), (1), and (2) denote the year before multiyear La Niña events, the first year, and the second year, respectively.

amplitude of La Niña during the event. For example, the 2010–2012 event had a stronger La Niña during the first year, while the 1998–2000 event had a stronger La Niña during the second year, and these events both led to a stronger TIW activity during the first year. On the other hand, the density difference anomaly between the equator and 6°N, corresponding to the density/temperature gradient between the equatorial tongue and the thermocline trough on the northern side of the equator (Figure 2a1), is shown (Figure 6c). Comparing the time series of the density difference anomaly and the TIW EKE anomaly, one can see that for every multiyear La Niña event including the 1998–2000 event, the density difference anomaly in the autumn of the first year is more positive than it in the autumn of the second year, which well coincides with the TIW EKE anomaly. As the density difference between the equator and 6°N is normally positive (Figure 6c), the stronger positive density difference anomaly during the first year compared to the second year indicates a larger density/temperature gradient. This demonstrates that the strong TIW activity during the first year is caused by the large temperature gradient, and TIW activity during the multiyear La Niña is controlled by the strength of the temperature gradient in the near-surface layer between the equatorial tongue and the thermocline trough on the north side of the equator, instead of the amplitude of La Niña, consistent with previous studies (e.g., Masina et al., 1999; Qiao & Weisberg, 1998; Wang et al., 2020; Z. Yu et al., 1995). On the other hand, previous research showed that stronger TIW activity may weaken the meridional temperature gradient by TIW-induced heat advection (e.g., Hansen & Paul, 1984; Imada & Kimoto, 2012; Jochum et al., 2007; Maillard, Boucharel, Stuecker, et al., 2022; Menkes et al., 2006). Therefore, there is a negative feedback between TIWs and meridional temperature gradient whereby the large temperature gradient in the first year causes the strong TIW activity, which in turn may reduce the temperature gradient by the strong TIW-induced heat flux.

One can also see that in the summer of the second years of most of the multiyear La Niña events except the 2016–2018 one, the density difference anomaly is negative, suggesting it is not only weaker than it in the summer of the first year but also weaker than its long-term mean. This results in the negative BC anomaly (Figures 3f1 and 4b) and thus contributes to the negative TIW EKE anomaly in the summer of the second year (Figure 4b), indicating that TIW activity is abnormally suppressed by the weakened temperature gradient via BC in the summer of the second year during most multiyear La Niña events.

Besides, one can also see that for most of the multiyear La Niña events except the 2020–2022 one, their first year is preceded by a strong El Niño (Niño-3.4 > 1 in December). Several previous studies have suggested that a strong El Niño event is a pre-onset condition for a following multi-year La Niña event (Hu et al., 2014; Iwakiri & Watanabe, 2021; Wu et al., 2019). A preceding strong El Niño event has the potential to trigger a Multiyear La Niña event. Subsequently, this multiyear La Niña event exerts a substantial strengthening effect on TIW activity during the first year, followed by a relatively weaker impact on TIW activity during the second year. This indirectly links the influence of a preceding strong El Niño event to the variations in TIW activity during the multiyear La Niña. In this way, the linkage between the complete ENSO cycle, which comprises of a strong El Niño event and a subsequent multiyear La Niña event, and TIW activity is established. Herein, in this study, the differences in the impact of the

multiyear La Niña event on TIW activity between the first and second years are identified and highlighted. This contributes to deepen our understanding of the interaction between the ENSO cycle and TIWs.

4. Summary and Discussion

In this work, we investigated the impact of the multiyear La Niña on TIWs and identified a unique feature of it, that is, stronger TIW activity during the first year compared to the second year. Using MWT and canonical transfer theory, the mechanism behind this feature is analyzed based on reanalysis data. Our findings reveal that during the first year, the equatorial cold tongue experiences anomalous strengthening, with cool SST anomalies confined to the equator. In contrast, the second year witnesses the spread of anomalously cool SST to off-equator regions, a weakened thermocline trough, and a less pronounced equatorial cold tongue compared to the first year. These disparities yield a stronger meridional density shear during the first year compared to the second year, resulting in a stronger baroclinic instability pathway, particularly in summer. On the other hand, the nSEC is stronger in the summer and autumn of the first year compared to the second year, caused by the stronger equatorial front north of the equator, resulting in a more intensified meridional velocity shear and a stronger barotropic instability energy pathway. Finally, the combination of the stronger barotropic and baroclinic instability energy pathways during the first year generates more TIW EKE from summer to winter. During the second year, the baroclinic instability energy pathway suppresses the TIW EKE in summer and provides a slight enhancement in autumn and winter, which is secondarily contributed by the weak barotropic instability energy pathway.

Our findings emphasize the importance of the impact of the thermodynamic structure of the equatorial cold tongue on TIWs during La Niña events. Our study also demonstrates that the impacts of ENSO on TIW activity are nonlinear. That is, the modulation of the interannual variability of TIW activity by ENSO cannot be expressed simply as a linear equation with the amplitude of ENSO events (i.e., Niño-3.4 index) as the independent variable. The interannual variability of TIW activity is modulated not only by the amplitude of ENSO but also by the longevity of ENSO events. The aforementioned feature can be seen as a response of TIWs to the temporal evolution of La Niña. Therefore, our findings suggest that it is important to classify the temporal evolution of La Niña events in order to analyze more accurately the impact of La Niña on TIWs.

On one hand, it has been reported that a meridionally expansive anomalous SST cooling pattern, potentially associated with North Pacific Meridional Mode and/or South Pacific Meridional Mode, is crucial for the redevelopment of La Niña during the second year (Hu et al., 2014; Iwakiri & Watanabe, 2021; Park et al., 2021; Shi et al., 2023). According to Hu et al. (2014), a strong La Niña in the first year is a precondition for its redevelopment in the following years. This ensures a strong westward propagating cooling temperature anomaly in the off-equatorial Pacific, suppressing the recharge process of ENSO, and thus favoring the persistence of the La Niña event. On the other hand, previous studies have shown that TIWs can exert significant meridional heat flux, heating the equator and cooling the off-equator regions, thereby reducing the meridional temperature gradient north of the equator (Maillard, Boucharel, Stuecker, et al., 2022; Szoeke et al., 2007; Xue et al., 2023). Given the substantial difference in the TIW activity between the first and second years of the multiyear La Niña event, it is worth investigating how the TIW-induced nonlinear dynamical heating (NDH) feedback varies during different years. As TIWs are more active during the first year, more heat is transported into the equatorial cold tongue, warming the SST on the equatorial eastern Pacific and cooling the SST on the off-equatorial regions, which may lead to a meridionally broader SST cooling over the tropical Pacific after the first year. This meridionally broader SST cooling may contribute to the redevelopment of La Niña in the second year. During the second year, the warming and cooling may be reduced due to the suppressed TIW activity, which may lead to a narrower region of SST cooling. This would not favor the redevelopment of La Niña in the third year. Therefore, if this proposed mechanism holds, TIWs may give feedback on the persistence of La Niña events by affecting the meridional structure of ENSO. Due to the small sample size of triple-dip La Niña events, in this study we did not analyze the TIW activity and its influence during this period. We leave this issue to future study with longer data.

Previous studies have indicated that the critical juncture for a La Niña shifting from recession in the spring of the second year to redevelopment typically transpires in the summer (Gao et al., 2022; Liu et al., 2023; Zheng et al., 2015). As can be seen in Figure 4, the most pronounced disparity in TIW activity between the first and second years also occurs in summer. Therefore, the reduction in NDH due to the suppressed TIW activity in the summer of the second year may contribute to the redevelopment of La Niña, increasing the likelihood of the double-dip La Niña event and improving its amplitude during the second year. This suggests another possible

pathway through which TIWs exert feedback on the temporal evolution of La Niña events via immediate heating. We look forward to extending this study to the investigation of the above potential feedback of TIWs on multiyear La Niña events.

Studying multiyear La Niña events is challenging due to the limited temporal coverage of available observations. This study primarily relies on the analysis of just five events. Using coupled GCMs to examine the TIWs variations related to the multiyear La Niña would be useful to understand the ability of models to simulate TIWs variations with respect to the observations, and allow for a comprehensive exploration of the feedback mechanism between TIWs and ENSO.

In this study, buoyancy conversion ($-b^1$) is used as the identification of baroclinic instability, as was done in many previous studies. However, it should be noted that while buoyancy conversion is important on its own, it represents a physical concept that may not invariably correspond to baroclinic instability, a point demonstrated in several real ocean studies, as exemplified by Liang and Robinson (2004). For instance, scenarios involving strain-induced frontogenesis can exhibit substantial conversion from eddy APE to EKE due to the establishment of a secondary overturning circulation. Such situations, however, may not necessarily imply the occurrence of baroclinic instability (McWilliams, 2016). Liang and Robinson (2007) has proved that, in the MWT-based framework, the canonical APE transfer from the mean flow to the perturbation field is related to the baroclinic instability in the classical sense (e.g., Pedlosky, 1979), with localized information retained. Considering the possible large deviation of the quasi-geostrophic definition of APE in the near-surface layer where TIWs are concentrated, making the canonical APE transfer not reliable, we look forward to using a more generalized APE, such as the one introduced by Holliday and Mcintyre (1981), and its associated canonical transfer to address the baroclinic generation of TIWs in future studies.

Data Availability Statement

The GLORYS and AVISO data sets are available at the Copernicus Marine and Environment Monitoring Service via https://data.marine.copernicus.eu/product/GLOBAL_MULTIYEAR_PHY_001_030/description and https://data.marine.copernicus.eu/product/SEALEVEL_GLO_PHY_L4_MY_008_047/description, respectively. HadISST is available at the Met Office Hadley Center via https://www.metoffice.gov.uk/hadobs/hadisst/. The MWT-based multiscale energetics analysis package can be downloaded at http://www.ncoads.cn/upload/202009/24/ms-eva_ocean.zip.

Acknowledgments
This study is supported by National Science Foundation of China (NSFC) (Grants 42230105, 42276017), by Southern Marine Science and Engineering Guangdong Laboratory (Zhuhai) (#313022005, #SML2023SP203), by Fudan University (#IDH2318009Y), by Shanghai B & R Joint Laboratory Project (Grant 22230750300), and by Shanghai International Science and Technology Partnership Project (Grant 21230780200).

References

An, S.-I. (2008). Interannual variations of the tropical ocean instability wave and ENSO. *Journal of Climate*, *21*(15), 3680–3686. https://doi.org/10.1175/2008JCLI1701.1

Boucharel, J., & Jin, F.-F. (2019). A simple theory for the modulation of tropical instability waves by ENSO and the annual cycle. *Tellus A: Dynamic Meteorology and Oceanography*, *72*(1), 1–14. https://doi.org/10.1080/16000870.2019.1700087

Chen, J., Yu, J.-Y., Chen, S., Wang, X., Xiao, Z., & Fang, S.-W. (2022). Tropical and subtropical Pacific sources of the asymmetric El Niño-La Niña decay and their future changes. *Geophysical Research Letters*, *49*(8), e2022GL097751. https://doi.org/10.1029/2022GL097751

Contreras, R. F. (2002). Long-term observations of tropical instability waves. *Journal of Physical Oceanography*, *32*(9), 2715–2722. https://doi.org/10.1175/1520-0485(2002)032<2715:LTOOTI>2.0.CO;2

DiNezio, P. N., & Deser, C. (2014). Nonlinear controls on the persistence of La Niña. *Journal of Climate*, *27*(19), 7335–7355. https://doi.org/10.1175/JCLI-D-14-00033.1

Feng, L., Zhang, R.-H., Wang, Z., & Chen, X. (2015). Processes leading to second-year cooling of the 2010–12 La Niña event, diagnosed using GODAS. *Advances in Atmospheric Sciences*, *32*(3), 424–438. https://doi.org/10.1007/s00376-014-4012-8

Gao, C., Chen, M., Zhou, L., Feng, L., & Zhang, R.-H. (2022). The 2020–2021 prolonged La Niña evolution in the tropical Pacific. *Science China Earth Sciences*, *65*(12), 2248–2266. https://doi.org/10.1007/s11430-022-9985-4

Geng, T., Jia, F., Cai, W., Wu, L., Gan, B., Jing, Z., et al. (2023). Increased occurrences of consecutive La Niña events under global warming. *Nature*, *619*(7971), 774–781. https://doi.org/10.1038/s41586-023-06236-9

Hansen, D. V., & Paul, C. A. (1984). Genesis and effects of long waves in the equatorial Pacific. *Journal of Geophysical Research*, *89*(C6), 10431–10440. https://doi.org/10.1029/JC089iC06p10431

He, W.-B., Yang, Y., & Liang, X. S. (2023). Mechanisms for generating and connecting the Yanai-mode and Rossby-mode tropical instability waves in the equatorial Pacific. *Deep Sea Research Part I: Oceanographic Research Papers*, *197*, 104041. https://doi.org/10.1016/j.dsr.2023.104041

Holliday, D., & Mcintyre, M. E. (1981). On potential energy density in an incompressible, stratified fluid. *Journal of Fluid Mechanics*, *107*(1), 221. https://doi.org/10.1017/S0022112081001742

Hu, Z.-Z., Kumar, A., Huang, B., Zhu, J., Zhang, R.-H., & Jin, F.-F. (2017). Asymmetric evolution of El Niño and La Niña: The recharge/discharge processes and role of the off-equatorial sea surface height anomaly. *Climate Dynamics*, *49*(7), 2737–2748. https://doi.org/10.1007/s00382-016-3498-4

Hu, Z.-Z., Kumar, A., Xue, Y., & Jha, B. (2014). Why were some La Niñas followed by another La Niña? *Climate Dynamics*, *42*(3–4), 1029–1042. https://doi.org/10.1007/s00382-013-1917-3

Imada, Y., & Kimoto, M. (2012). Parameterization of tropical instability waves and examination of their impact on ENSO characteristics. *Journal of Climate*, *25*(13), 4568–4581. https://doi.org/10.1175/JCLI-D-11-00233.1

Iwakiri, T., & Watanabe, M. (2021). Mechanisms linking multi-year La Niña with preceding strong El Niño. *Scientific Reports*, *11*(1), 17465. https://doi.org/10.1038/s41598-021-96056-6

Izumo, T. (2005). The equatorial undercurrent, meridional overturning circulation, and their roles in mass and heat exchanges during El Niño events in the tropical Pacific Ocean. *Ocean Dynamics*, *55*(2), 110–123. https://doi.org/10.1007/s10236-005-0115-1

Jean-Michel, L., Eric, G., Romain, B.-B., Gilles, G., Angélique, M., Marie, D., et al. (2021). The Copernicus global 1/12° oceanic and sea ice GLORYS12 reanalysis. *Frontiers in Earth Science*, *9*. https://doi.org/10.3389/feart.2021.698876

Jochum, M., Cronin, M. F., Kessler, W. S., & Shea, D. (2007). Observed horizontal temperature advection by tropical instability waves. *Geophysical Research Letters*, *34*(9), L09604. https://doi.org/10.1029/2007GL029416

Kessler, W. S. (2002). Is ENSO a cycle or a series of events? *Geophysical Research Letters*, *29*(23), 40-1–40-4. https://doi.org/10.1029/2002GL015924

Legeckis, R. (1977). Long waves in the eastern equatorial Pacific ocean: A view from a geostationary satellite. *Science*, *197*(4309), 1179–1181. https://doi.org/10.1126/science.197.4309.1179

Liang, X. S. (2016). Canonical transfer and multiscale energetics for primitive and quasigeostrophic atmospheres. *Journal of the Atmospheric Sciences*, *73*(11), 4439–4468. https://doi.org/10.1175/JAS-D-16-0131.1

Liang, X. S., & Anderson, D. G. M. (2007). Multiscale window transform. *Multiscale Modeling and Simulation*, *6*(2), 437–467. https://doi.org/10.1137/06066895X

Liang, X. S., & Robinson, A. R. (2004). A study of the Iceland-Faeroe frontal variability using the multiscale energy and vorticity analysis. *Journal of Physical Oceanography*, *34*(12), 2571–2591. https://doi.org/10.1175/jpo2661.1

Liang, X. S., & Robinson, A. R. (2005). Localized multiscale energy and vorticity analysis: I. Fundamentals. *Dynamics of Atmospheres and Oceans*, *38*(3–4), 195–230. https://doi.org/10.1016/j.dynatmoce.2004.12.004

Liang, X. S., & Robinson, A. R. (2007). Localized multi-scale energy and vorticity analysis: II. Finite-amplitude instability theory and validation. *Dynamics of Atmospheres and Oceans*, *44*(2), 51–76. https://doi.org/10.1016/j.dynatmoce.2007.04.001

Liu, F., Zhang, W., Jin, F.-F., Jiang, F., Boucharel, J., & Hu, S. (2023). New insights into multi-year La Niña dynamics from the perspective of a near-annual ocean process. *Journal of Climate*, *1*(aop), 1–35. https://doi.org/10.1175/JCLI-D-22-0505.1

Lorenz, E. N. (1955). Available potential energy and the maintenance of the general circulation. *Tellus*, *7*(2), 157–167. https://doi.org/10.3402/tellusa.v7i2.8796

Lyman, J. M., Johnson, G. C., & Kessler, W. S. (2007). Distinct 17- and 33-day tropical instability waves in subsurface observations. *Journal of Physical Oceanography*, *37*(4), 855–872. https://doi.org/10.1175/jpo3023.1

Maillard, L., Boucharel, J., & Renault, L. (2022). Direct and rectified effects of tropical instability waves on the eastern tropical Pacific mean state in a regional ocean model. *Journal of Physical Oceanography*, *52*(8), 1817–1834. https://doi.org/10.1175/JPO-D-21-0300.1

Maillard, L., Boucharel, J., Stuecker, M. F., Jin, F.-F., & Renault, L. (2022). Modulation of the eastern equatorial Pacific seasonal cycle by tropical instability waves. *Geophysical Research Letters*, *49*(23), e2022GL100991. https://doi.org/10.1029/2022GL100991

Masina, S., Philander, S. G. H., & Bush, A. B. G. (1999). An analysis of tropical instability waves in a numerical model of the Pacific Ocean: 2. Generation and energetics of the waves. *Journal of Geophysical Research*, *104*(C12), 29637–29661. https://doi.org/10.1029/1999jc900226

McPhaden, M. J. (1993). Trade wind fetch-related variations in equatorial undercurrent depth, speed, and transport. *Journal of Geophysical Research*, *98*(C2), 2555–2559. https://doi.org/10.1029/92JC02683

McWilliams, J. C. (2016). Submesoscale currents in the ocean. *Proceedings of the Royal Society A: Mathematical, Physical and Engineering Sciences*, *472*(2189), 20160117. https://doi.org/10.1098/rspa.2016.0117

Menkes, C. E. R., Vialard, J. G., Kennan, S. C., Boulanger, J.-P., & Madec, G. V. (2006). A modeling study of the impact of tropical instability waves on the heat budget of the eastern equatorial Pacific. *Journal of Physical Oceanography*, *36*(5), 847–865. https://doi.org/10.1175/JPO2904.1

Ohba, M., & Ueda, H. (2009). Role of nonlinear atmospheric response to SST on the asymmetric transition process of ENSO. *Journal of Climate*, *22*(1), 177–192. https://doi.org/10.1175/2008JCLI2334.1

Okumura, Y. M., & Deser, C. (2010). Asymmetry in the duration of El Niño and La Niña. *Journal of Climate*, *23*(21), 5826–5843. https://doi.org/10.1175/2010JCLI3592.1

Okumura, Y. M., DiNezio, P., & Deser, C. (2017). Evolving impacts of multiyear La Niña events on atmospheric circulation and U.S. Drought. *Geophysical Research Letters*, *44*(22), 11614–11623. https://doi.org/10.1002/2017GL075034

Okumura, Y. M., Ohba, M., Deser, C., & Ueda, H. (2011). A proposed mechanism for the asymmetric duration of El Niño and La Niña. *Journal of Climate*, *24*(15), 3822–3829. https://doi.org/10.1175/2011JCLI3999.1

Park, J.-H., An, S.-I., Kug, J.-S., Yang, Y.-M., Li, T., & Jo, H.-S. (2021). Mid-latitude leading double-dip La Niña. *International Journal of Climatology*, *41*(S1), E1353–E1370. https://doi.org/10.1002/joc.6772

Pedlosky, J. (1979). *Geophysical fluid dynamics*. Springer US. https://doi.org/10.1007/978-1-4684-0071-7

Philander, S. G. H. (1978). Instabilities of zonal equatorial currents, 2. *Journal of Geophysical Research*, *83*(C7), 3679–3682. https://doi.org/10.1029/JC083iC07p03679

Qiao, L., & Weisberg, R. H. (1995). Tropical instability wave kinematics: Observations from the tropical instability wave experiment. *Journal of Geophysical Research*, *100*(C5), 8677–8693. https://doi.org/10.1029/95JC00305

Qiao, L., & Weisberg, R. H. (1998). Tropical instability wave energetics: Observations from the tropical instability wave experiment. *Journal of Physical Oceanography*, *28*(2), 345–360. https://doi.org/10.1175/1520-0485(1998)028<0345:TIWEOF>2.0.CO;2

Rayner, N. A., Parker, D. E., Horton, E. B., Folland, C. K., Alexander, L. V., Rowell, D. P., et al. (2003). Global analyses of sea surface temperature, sea ice, and night marine air temperature since the late nineteenth century. *Journal of Geophysical Research*, *108*(D14), 4407. https://doi.org/10.1029/2002JD002670

Shi, L., Ding, R., Hu, S., Li, X., & Li, J. (2023). Extratropical impacts on the 2020–2023 triple-dip La Niña event. *Atmospheric Research*, *294*, 106937. https://doi.org/10.1016/j.atmosres.2023.106937

von Storch, J.-S., Eden, C., Fast, I., Haak, H., Hernández-Deckers, D., Maier-Reimer, E., et al. (2012). An estimate of the Lorenz energy cycle for the World ocean based on the STORM/NCEP simulation. *Journal of Physical Oceanography*, *42*(12), 2185–2205. https://doi.org/10.1175/JPO-D-12-079.1

de Szoeke, S. P., Xie, S.-P., Miyama, T., Richards, K. J., & Small, R. J. O. (2007). What maintains the SST front north of the eastern Pacific equatorial cold tongue? *Journal of Climate*, *20*(11), 2500–2514. https://doi.org/10.1175/JCLI4173.1

Traon, P. Y. L., Nadal, F., & Ducet, N. (1998). An improved mapping method of multisatellite altimeter data. *Journal of Atmospheric and Oceanic Technology*, *15*(2), 522–534. https://doi.org/10.1175/1520-0426(1998)015<0522:AIMMOM>2.0.CO;2

Tuchen, F. P., Brandt, P., Claus, M., & Hummels, R. (2018). Deep intraseasonal variability in the central equatorial Atlantic. *Journal of Physical Oceanography*, *48*(12), 2851–2865. https://doi.org/10.1175/JPO-D-18-0059.1

Vialard, J., Menkes, C., Boulanger, J.-P., Delecluse, P., Guilyardi, E., McPhaden, M. J., & Madec, G. (2001). A model study of oceanic mechanisms affecting equatorial Pacific sea surface temperature during the 1997–98 El Niño. *Journal of Physical Oceanography*, *31*(7), 1649–1675. https://doi.org/10.1175/1520-0485(2001)031<1649:AMSOOM>2.0.CO;2

Wang, M., Du, Y., Qiu, B., Cheng, X., Luo, Y., Chen, X., & Feng, M. (2017). Mechanism of seasonal eddy kinetic energy variability in the eastern equatorial Pacific Ocean. *Journal of Geophysical Research: Oceans*, *122*(4), 3240–3252. https://doi.org/10.1002/2017JC012711

Wang, M., Du, Y., Qiu, B., Xie, S.-P., & Feng, M. (2019). Dynamics on seasonal variability of EKE associated with TIWs in the eastern equatorial Pacific Ocean. *Journal of Physical Oceanography*, *49*(6), 1503–1519. https://doi.org/10.1175/jpo-d-18-0163.1

Wang, M., Xie, S.-P., Shen, S. S. P., & Du, Y. (2020). Rossby and Yanai modes of tropical instability waves in the equatorial Pacific Ocean and a diagnostic model for surface currents. *Journal of Physical Oceanography*, *50*(10), 3009–3024. https://doi.org/10.1175/jpo-d-20-0063.1

Weisberg, R. H., & Weingartner, T. J. (1988). Instability waves in the equatorial Atlantic Ocean. *Journal of Physical Oceanography*, *18*(11), 1641–1657. https://doi.org/10.1175/1520-0485(1988)018<1641:IWITEA>2.0.CO;2

Wu, X., Okumura, Y. M., & DiNezio, P. N. (2019). What controls the duration of El Niño and La Niña events? *Journal of Climate*, *32*(18), 5941–5965. https://doi.org/10.1175/JCLI-D-18-0681.1

Xue, A., Jin, F.-F., Zhang, W., Boucharel, J., & Kug, J.-S. (2023). Parameterizing the nonlinear feedback on ENSO from tropical instability waves (TIWs) by nonlinear eddy thermal diffusivity. *Climate Dynamics*, *61*(7–8), 3525–3540. https://doi.org/10.1007/s00382-023-06744-4

Yang, Y., & Liang, X. S. (2019). Spatiotemporal variability of the global ocean internal processes inferred from satellite observations. *Journal of Physical Oceanography*, *49*(8), 2147–2164. https://doi.org/10.1175/JPO-D-18-0273.1

Yu, J.-Y., & Liu, W. T. (2003). A linear relationship between ENSO intensity and tropical instability wave activity in the eastern Pacific ocean: Relationship between ENSO and TIWS. *Geophysical Research Letters*, *30*(14), 1735. https://doi.org/10.1029/2003GL017176

Yu, Z., McCreary, J. P., & Proehl, J. A. (1995). Meridional asymmetry and energetics of tropical instability waves. *Journal of Physical Oceanography*, *25*(12), 2997–3007. https://doi.org/10.1175/1520-0485(1995)025<2997:MAAEOT>2.0.CO;2

Zheng, F., Feng, L., & Zhu, J. (2015). An incursion of off-equatorial subsurface cold water and its role in triggering the "double dip" La Niña event of 2011. *Advances in Atmospheric Sciences*, *32*(6), 731–742. https://doi.org/10.1007/s00376-014-4080-9

Zhu, T., & Yu, J.-Y. (2022). A shifting tripolar pattern of Antarctic sea ice concentration anomalies during multi-year La Niña events. *Geophysical Research Letters*, *49*(23), e2022GL101217. https://doi.org/10.1029/2022GL101217